Spectrally-resolved UV photodesorption of CH4 in pure and layered ices

Rémi Dupuy, Mathieu Bertin, Géraldine Féraud, Xavier Michaut, Pascal Jeseck, Mikhail Doronin, Laurent Philippe, C Romanzin, J.-H Fillion

A&A 603, A61 (2017)
DOI: 10.1051/0004-6361/201730772

Astronomy & Astrophysics

Spectrally-resolved UV photodesorption of CH_4 in pure and layered ices

R. Dupuy[1], M. Bertin[1], G. Féraud[1], X. Michaut[1], P. Jeseck[1], M. Doronin[1], L. Philippe[1], C. Romanzin[2], and J.-H. Fillion[1]

[1] Laboratoire d'Étude du Rayonnement et de la Matière en Astrophysique et Atmosphères (LERMA), Sorbonne Universités, UPMC Univ. Paris 06, Observatoire de Paris, PSL Research University, CNRS UMR 8112, 75005 Paris, France
e-mail: remi.dupuy@obspm.fr
[2] Laboratoire de Chimie Physique (LCP), CNRS UMR 8000, Univ. Paris Sud, 91400 Orsay, France

Received 13 March 2017 / Accepted 14 April 2017

ABSTRACT

Context. Methane is among the main components of the ice mantles of interstellar dust grains, where it is at the start of a rich solid-phase chemical network. Quantification of the photon-induced desorption yield of these frozen molecules and understanding of the underlying processes is necessary to accurately model the observations and the chemical evolution of various regions of the interstellar medium.
Aims. This study aims at experimentally determining absolute photodesorption yields for the CH_4 molecule as a function of photon energy. The influence of the ice composition is also investigated. By studying the methane desorption from layered CH_4:CO ice, indirect desorption processes triggered by the excitation of the CO molecules are monitored and quantified.
Methods. Tunable monochromatic vacuum ultraviolet light (VUV) light from the DESIRS beamline of the SOLEIL synchrotron is used in the 7–13.6 eV (177–91 nm) range to irradiate pure CH_4 or layers of CH_4 deposited on top of CO ice samples. The release of species in the gas phase is monitored by quadrupole mass spectrometry, and absolute photodesorption yields of intact CH_4 are deduced.
Results. CH_4 photodesorbs for photon energies higher than ~9.1 eV (~136 nm). The photodesorption spectrum follows the absorption spectrum of CH_4, which confirms a desorption mechanism mediated by electronic transitions in the ice. When it is deposited on top of CO, CH_4 desorbs between 8 and 9 eV with a pattern characteristic of CO absorption, indicating desorption induced by energy transfer from CO molecules.
Conclusions. The photodesorption of CH_4 from pure ice in various interstellar environments is around $2.0 \pm 1.0 \times 10^{-3}$ molecules per incident photon. Results on CO-induced indirect desorption of CH_4 provide useful insights for the generalization of this process to other molecules co-existing with CO in ice mantles.

Key words. astrochemistry – ISM: abundances – ISM: molecules – molecular processes – methods: laboratory: solid state

1. Introduction

In cold and dense regions of the interstellar medium (ISM), such as dense molecular clouds or protoplanetary disks mid-planes, interstellar dust grains are coated with an ice mantle, composed of molecules either accreted from the gas phase or formed directly on the surface. Due to the low temperatures in these regions (~10 K) thermal desorption is negligible, and the exchanges between the gas phase and those icy mantles are thus driven by non-thermal processes. Among them, desorption stimulated by UV photons emitted by nearby stars or secondary UV photons emitted by excited molecules is thought to play a significant role. Laboratory experiments in the last few years have aimed at quantitatively and qualitatively describing such photon-stimulated desorption (PSD) processes for astrophysically relevant ice analogs, (see e.g., Öberg et al. 2009; Hama et al. 2009; Fayolle et al. 2011; Yuan & Yates 2014; Martín-Doménech et al. 2016) which is required in order to explain the observations of molecule abundances in the gas and solid phases and to accurately model the chemical evolution in the concerned regions of the ISM. Photodesorption can also be relevant in other astrophysical media; it has been considered as one of the possible space-weathering agents of solar system bodies (Bennett et al. 2013).

CH_4 has been observed toward protostellar objects (Dartois et al. 1998; Boogert et al. 1998) in the gas and solid phase, with an estimated CH_4 gas to ice ratio of 0.3–0.5. CH_4 formation was proposed to occur on grains, and it was found to exist in polar ices containing H_2O and CH_3OH (Boogert et al. 1998). CH_4 is also detected in ices toward young stellar objects (YSOs) with a typical abundance of 1–10% with respect to H_2O, while in quiescent clouds and cores only an upper limit of <3% is found (Boogert et al. 2015). In cometary ices, the typical abundance relative to H_2O is 1% (Mumma & Charnley 2011), lower than in the previously cited environments. The observations toward YSOs suggest that the dominant formation mechanism of CH_4 in the ISM is through hydrogenation of atomic C at the surface of grains (Öberg et al. 2008). Such a mechanism has been experimentally confirmed (Hiraoka et al. 1998). This implies that desorption from grains constitutes the main source of CH_4 in the gas phase. CH_4 abundances in the gas phase are poorly known mainly because of its lack of a permanent dipole moment, meaning that no detection is possible at radio wavelengths (Boogert et al. 2004). This lack

of observational constraints makes it even more crucial to have accurate modeling parameters when assessing the available reservoir of CH_4. Indeed, methane is included in gas-grain models for cold clouds, disks, and illuminated regions such as photon-dominated regions (PDR) (Ruaud et al. 2016; Kalvans 2015; Hollenbach et al. 2009; Garrod & Pauly 2011; Cleeves et al. 2016).

Evaporation of CH_4 from the grain mantles is the first step of a gas phase chemistry leading to the formation of carbon chains (as in protostars and protoplanetary disks, see e.g., Sakai & Yamamoto 2013; Aikawa & Nomura 2006; Hassel et al. 2008). Moreover, photodissociation products of methane initiate a chemical network that has been well experimentally studied in the gas phase, due to the fact that it is also very relevant to planetary science (Romanzin et al. 2005; Gans et al. 2011; Smith & Raulin 1999).

In the solid phase, CH_4 is also at the start of a rich chemical network. Laboratory experiments on the processing of pure CH_4 ice with energetic particles (Kaiser & Roessler 1998; Baratta et al. 2003; Bennett et al. 2006; de Barros et al. 2011) and UV photons (Lo et al. 2015; Bossa et al. 2015) as well as mixes with other astrophysically relevant molecules such as H_2O (Öberg et al. 2010; Hodyss et al. 2009), N_2 (Wu et al. 2012), CO (Maity et al. 2014) or N_2:CO (Hodyss et al. 2011) have yielded a great variety of products.

Non-thermal desorption/sputtering of methane by energetic ions and electrons has already been extensively studied (Johnson et al. 2013, and references therein). This is not the case for UV irradiation. Cruz-Diaz et al. (2016) observed CH_4 desorption when UV-irradiating a pure methanol ice, demonstrating a pathway to the release of methane in the gas phase other than direct methane photodesorption. However, in their study of pure CH_4 ice, they did not observe intact CH_4 photodesorption (Cruz-Diaz 2015). Instead, desorption of photoproducts such as C_2H_4 was seen. A recent study by Martín-Doménech et al. (2016) has also shown that a part of the reaction products (e.g., H_2CO) initiated by the methane photodissociation in mixed CH_4:H_2O ices is released in the gas phase during UV irradiation. However, they did not observe intact CH_4 photodesorption either. The present study is therefore, to our knowledge, the first report of CH_4 photodesorption from pure CH_4 ice. We have focused on the desorption of the intact CH_4 molecule, and obtained absolute photodesorption yields as a function of the UV photon energy between 7 and 13.6 eV. This allows one to derive photodesorption yields for any given astrophysically relevant UV field. In order to test the influence of the environment of the molecules on photodesorption, we also investigated the desorption of layers of CH_4 deposited on top of CO ice. CO is a very abundant component of interstellar ices, and has a high photodesorption yield (Fayolle et al. 2011), therefore its ability to indirectly induce desorption of other molecules (Bertin et al. 2013) could have important astrophysical implications.

2. Methods

Experiments were performed in the SPICES (Surface Processes & ICES) set-up, which has previously been described in detail (Doronin et al. 2015). It consists of an ultra-high vacuum (UHV) chamber with a base pressure of typically 10^{-10} mBar, within which a polycrystalline gold surface is mounted on a rotatable cold head that can be cooled down to ~10 K using a closed cycle helium cryostat. Ices of $^{13}CH_4$ (Eurisotop, >99.9% purity in ^{13}C) and CO (Air liquide, >99.9% purity) are dosed by exposing the cold surface (10 K) to a partial pressure of gas using a tube positioned a few millimeters away from the surface, allowing rapid growth without increasing the chamber pressure to more than a few 10^{-9} mBar. Ice thicknesses are controlled with a precision better than 1 monolayer (ML) via a calibration using the temperature programmed desorption (TPD) technique, as detailed in Doronin et al. (2015). The release of species in the gas phase is monitored by means of a quadrupole mass spectrometer (QMS).

The chamber is then coupled to the undulator-based DESIRS beamline (Nahon et al. 2012) at the SOLEIL synchrotron facility, which provides a monochromatic, tunable radiation beam hitting the sample at 45° incidence. The coupling is window-free to prevent cut-off of the higher energy photons. To acquire photodesorption spectra, the narrow bandwidth (~25 meV) output of a grating monochromator is continuously scanned between 7 and 14 eV. Higher harmonics of the undulator are suppressed using a Krypton gas filter. Typical photon fluxes as measured with a calibrated AXUV photodiode depend on the photon energy and vary between 5×10^{12} and 17×10^{12} photons cm^{-2} s^{-1}.

During the photon energy scan, the relative amount of photodesorbed molecules is recorded by the QMS. Each 25 meV photon energy step lasts about 5 s, which is sufficiently higher than the dwell time of the QMS (0.5 s). A typical scan thus lasts around 20 min, which corresponds to a total photon dose of ~10^{16} photons cm^{-2}.

Once corrected from the background contribution and divided by the photon flux, the QMS signal I_i corresponds to the relative efficiency of photodesorption as a function of photon energy. This signal can then be converted to absolute photodesorption yields. For a given species i, the absolute photodesorption yield Y_i (in molecules per incident photons) is proportional to the signal I_i at the m/z ratio of species i, such that $Y_i = f_i \times I_i$. f_i can be further expanded into $f_i = g \times h_i$ where g is a factor intrinsic to the QMS and the geometry of our set-up, and h_i is a factor specific to each species i. In the case of CO, f_{CO} can be obtained by comparing the photodesorption signal of a pure CO ice taken during the experimental runs to the well-known CO absolute photodesorption yields (Fayolle et al. 2011). This calibration is then used as a basis to derive the proportionality coefficients f_i of the other species. This is done by correcting f_{CO} by molecule-dependent factors such as the electron-impact ionization cross-section, which characterizes the fact that CO and species i are not ionized with the same efficiency by the ionization chamber, and the apparatus function of our QMS, which characterizes the fact that ions with a different m/z ratio are not detected with the same efficiency by the QMS. Thus, for CH_4, we have:

$$Y_{CH_4} = f_{CH_4} \times I_{CH_4} = f_{CO} \times \frac{\sigma(CH_4^+/CH_4)}{\sigma(CO^+/CO)} \times \frac{AF(CH_4)}{AF(CO)} \times I_{CH_4} \quad (1)$$

where $\sigma(i^+/i)$ is the partial electron-impact ionization cross-section of the i^+ ion relative to its parent molecule i, and AF(i) is the apparatus function of our QMS for species i (AF(CO) is set to 1).

Until now we assumed that the QMS signal at a given m/z ratio originated from a single species i. However, due to cracking in the QMS, an ion can originate from different parent molecules, and the signal has to be corrected from the contribution of the irrelevant parent molecules. For example in our case, the signal measured on mass 16 (corresponding here to $^{13}CH_3^+$) could be originating from either desorbed CH_3 radicals or from desorbed CH_4 molecules that are cracked in the ionization chamber of the QMS. Thus in order to know if there is a signal originating from desorbing CH_3, the latter contribution has to be substracted using

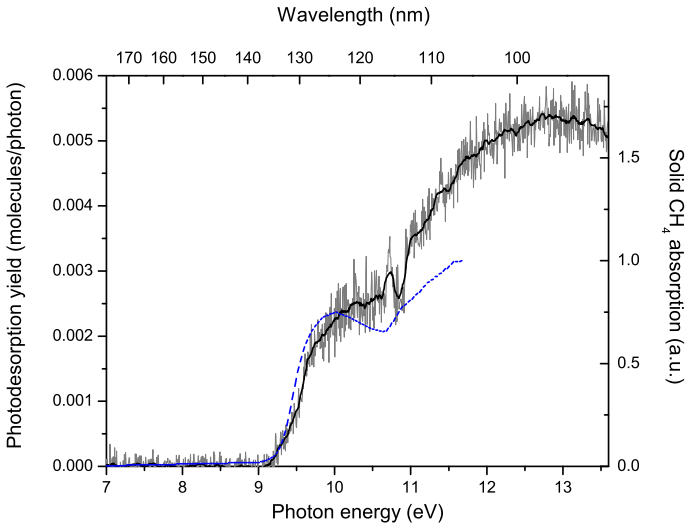

Fig. 1. $^{13}CH_4$ photodesorption spectrum of a 20 ML thick $^{13}CH_4$ ice at 10 K between 7 and 13.6 eV. The blue dotted line (right axis) is the absorption spectrum of pure CH_4 adapted from Wu et al. (2012).

the partial ionization cross-sections of CH_4 and CH_3:

$$I_{CH_3} = I_{CH_3^+} - \frac{\sigma(CH_3^+/CH_4)}{\sigma(CH_4^+/CH_4)} \times \frac{AF(CH_3)}{AF(CH_4)} \times I_{CH_4} \quad (2)$$

where $I_{CH_3^+}$ is the total signal measured on mass channel 16 and I_{CH_3} is the signal originating from desorbing CH_3 (so far we have assumed that ions in the QMS had only one parent molecule, i.e., $I_i = I_{i^+}$).

For similar reasons, $^{13}CH_4$ was used in order to distinguish it in mass spectrometry from O^+ fragments (m/z = 16, same as $^{12}CH_4^+$) originating from the cracking of CO in the QMS, during CH_4 layered on CO experiments. This consideration also brings up the possibility that part of the CH_4^+ signal detected originates not from desorbing CH_4 but from larger molecules formed by photolysis of the ice and photodesorbed. However, the expected photolysis products of solid CH_4, such as C_2H_2, C_2H_4, C_2H_6 or larger hydrogenated carbon-chains (e.g., Lo et al. 2015) only lead to negligible CH_4^+ signal by electron-impact ionization at 70 eV[1]. We have therefore made the assumption that desorption of possible photoproducts from the solid methane does not participate to the recorded CH_4^+ signal, that is thus only related to the desorption of intact CH_4.

The calibration of our spectra is done using the apparatus function of our QMS as determined by calibration experiments using several molecules with well-known electron-impact cracking patterns and the partial electron-impact ionization cross-sections at 70 eV found in Tian & Vidal (1998) for CH_4 and CO. While the uncertainties on the relative photodesorption spectra are only due to experimental noise, background substraction and photon flux uncertainties, this calibration method introduces much larger uncertainties on the absolute photodesorption yields. We estimate a systematic 50% uncertainty on all the absolute photodesorption yields given for CH_4 hereafter.

3. Results

3.1. Pure CH_4 ice

Figure 1 shows the photodesorption yield as a function of photon energy of CH_4 from a pure, 20 ML-thick CH_4 ice. There is a threshold at 9.1 eV under which desorption is below our detection limit. A broad peak is centered around 10 eV, then desorption steadily increases from 10.5 eV onwards, with a maximum around 13 eV. The absorption spectrum of pure CH_4 adapted from Wu et al. (2012) is given for comparison, and it matches fairly well the desorption profile, at least until their cut-off energy. The 10 eV broad feature is less well defined in our desorption spectrum. The absorption spectrum taken by Koch & Skibowski (1971), which has a higher energy cut-off, suggests that the absorption continues to increase until around 14 eV. We did not use that spectrum here because it has a 0.5 eV red-shift compared with the spectrum from Wu et al. (2012). This is probably because of different experimental conditions; the spectrum by Koch & Skibowski (1971) was taken at 30K, where CH_4 is expected to be crystalline rather than amorphous (Hudson et al. 2015). The spectrum from Cruz-Diaz et al. (2014b), taken at 10 K under UHV conditions as well and recorded at energies lower than 10.3 eV, agrees with the one by Wu et al. (2012).

The absorption spectrum of CH_4 in the gas phase has a threshold at 8.5 eV and two, rather than one, broad features centered at 9.7 and 10.5 eV. These two features have been attributed to the $1t_2$ -> 3s Rydberg transitions of respectively the D_{2d} and C_{3v} symmetries of the ion (Au et al. 1993). As discussed in Robin (1974), the equivalent feature at 10 eV in the solid spectrum can thus probably be attributed to excitons, which is also supported by calculations (Kunz 1983). The fact that the desorption spectrum matches the absorption spectrum and the attributions discussed here is clear evidence that desorption is initiated by an electronic transition. After 11 eV, the absorption of gas-phase CH_4 continues to increase as in the solid phase, although there are no clearly discernible features. Virtual valence orbitals are thought to be above the first ionization potential at 13.6 eV, therefore the absorption in this region has been attributed to overlapping Rydberg transitions. The ionization threshold of CH_4 in the gas phase is at 12.5 eV (Kameta et al. 2002) and is redshifted by 1.2 eV in the solid phase (Himpsel et al. 1975) which puts it at 11.3 eV. In the gas phase, Kameta et al. (2002) have measured the relative weight of neutral dissociation and ionization in the absorption of CH_4. Below the ionization threshold, there is only neutral dissociation, but as the ionization channel opens, neutral dissociation decreases until only ionization processes occur, at 16 eV. Therefore, the desorption mechanisms at the origin of the 10 eV feature are likely different from those responsible for the desorption signal above 11 eV.

We have observed evidence of aging of the CH_4 ice: when it has already been processed by VUV irradiation, the desorption yield decreases. This means that despite our low fluence, which usually allows us to probe desorption processes without affecting the ice significantly, photochemistry and/or ice restructuration (due to release of energy in the bulk) must play a role. Systematic studies of the effect of processing will be required to understand the exact nature of the aging effect and how much it affects photodesorption. In the meantime we only present results for "fresh" ice.

The masses corresponding to the CH_3, CH_2, and CH fragments were also monitored during the photon irradiation. Once corrected from the cracking of desorbing CH_4 in the ionization chamber of the QMS, the remaining signals fall below our sensitivity level, meaning that we are unable to observe the desorption of these radicals if they do desorb. This is despite the fact that at least the CH_3 radical fragment has been detected as trapped in photolyzed methane ice (Lo et al. 2015) and matrix-isolated methane (Milligan & Jacox 1967).

[1] http://webbook.nist.gov/chemistry/

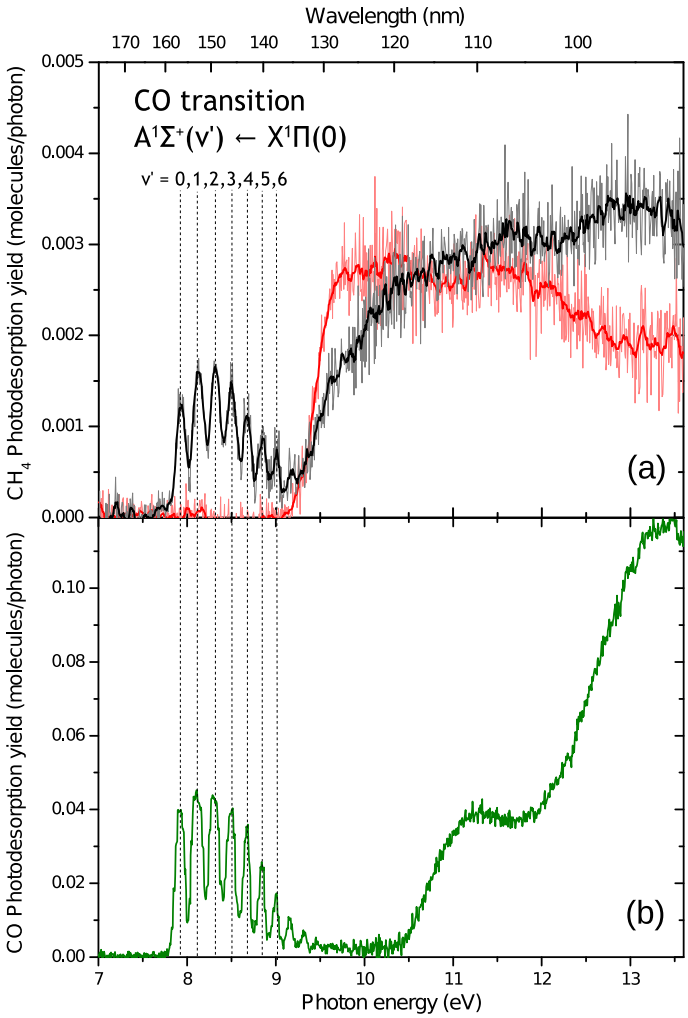

Fig. 2. a) $^{13}CH_4$ photodesorption spectrum of 1 ML (black trace) and 3 ML (red trace) of $^{13}CH_4$ on top of 20 ML of CO ice at 10 K, between 7 and 13.6 eV. **b)** CO photodesorption spectrum of a 20 ML thick pure CO ice at 10 K. Electronic transitions are indicated by vertical dashed lines.

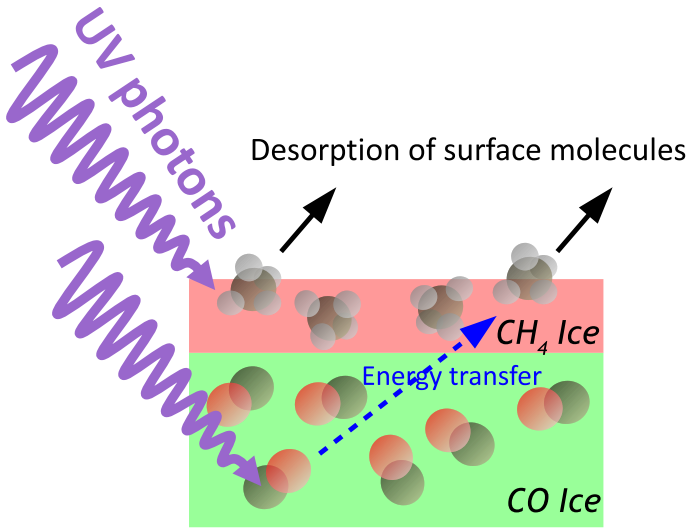

Fig. 3. Simplified scheme of the two desorption mechanisms at play: direct desorption of surface $^{13}CH_4$, and indirect desorption of surface $^{13}CH_4$ after energy transfer from underlying CO molecules.

3.2. CH_4 on top of CO ice

Figure 2b shows the photodesorption spectrum of a pure 20 ML-thick CO ice (measured at $m/z = 28$ CO). Between 8 and 9 eV, this spectrum shows very characteristic peaks that correspond to the vibrational levels of the $A^1\Sigma \leftarrow X^1\Pi$ electronic transition of condensed CO. This feature allowed for labeling of the desorption at these energies as a DIET (Desorption Induced by Electronic Transition) process (Fayolle et al. 2011). It was later found that desorption in this region could be in great part attributed to an indirect mechanism (Bertin et al. 2012). "Indirect" here means that the desorbing molecule is not the one that has absorbed a photon. Instead, a CO molecule in the first few subsurface monolayers of the ice is excited, then an energy transfer induces the desorption of another, surface-located CO molecule. Above 10.5 eV, two broad features are observed. The CO desorption mechanism for these two features is not clear, since in this region electronic states are dissociative and ionization can occur at 12.5 eV and above, which opens many more possibilities other than a "simple" DIET mechanism, such as photo-electron induced desorption or neutral-neutral or ion-neutral recombination chemistry.

Figure 2a shows the photodesorption spectrum of 1 ML of CH_4 deposited on top of 20 ML of CO. The desorption profile is significantly changed as compared with the pure CH_4 ice. Between 8 and 9 eV, where CH_4 does not desorb in the pure ice case (Fig. 1), desorption peaks are observed that correspond to the signature peaks of CO excitation. This is a clear indication that an indirect desorption mechanism is at play. This indirect mechanism is schematized in Fig. 3: the excitation of a sub-surface CO molecule is followed by an energy transfer to a CH_4 molecule at the surface, which then desorbs. The principle is identical to the indirect mechanism that was found in pure CO, and we discuss in Sect. 4.2 the generalization of this "CO-induced" desorption mechanism. The photodesorption of CH_4 on CO is a superimposition of the pure CO (Fig. 2b) and pure CH_4 (Fig. 1) profiles; while the peaks between 8 and 9 eV are entirely due to CO-induced indirect desorption, desorption around 10 eV unambiguously corresponds to CH_4 absorption and subsequent desorption, since CO absorption (and desorption) is very weak in this region. In the region above 11 eV, both molecules absorb significantly and they probably both contribute to the observed desorption of CH_4, although no clear features can be discerned.

In Fig. 2a, also represented is the photodesorption spectrum of 3 ML of CH_4 deposited on top of 20 ML of CO. At this thickness, no CO-induced desorption is seen at all, and the spectrum looks like the photodesorption spectrum of 20 ML of CH_4 below 10.5 eV. In this system, indirect desorption is negligible if more than 3 ML of CH_4 are deposited on top of CO ice. Both the 1 and 3 ML of CH_4 on CO exhibit lower desorption yields in the region above 11 eV than in the case of the pure 20 ML ice, which suggests either a thickness dependence of the desorption in this region or that the ageing effect mentioned earlier is more efficient in thin layers. In this latter case, the ice could have aged as the scan occurred, resulting in a lower yield at high energies. The yield at high energy of the 3 ML layer is even lower than the 1 ML one, which is evidence that there is a contribution, although almost structureless, of CO-induced desorption in the latter case.

4. Discussion

4.1. Photodesorption mechanisms in pure CH_4 ices

In the relatively more simple case of molecules that do not dissociate upon VUV irradiation (e.g., CO under 10 eV, N_2), photodesorption has been attributed to a DIET process, which as discussed above can be direct or indirect, where the molecule stays intact throughout the process (Bertin et al. 2012, 2013). Such a process cannot be excluded here, but the fact that the energy threshold for dissociation of CH_4 in the gas phase is much lower than the photon energy (Gans et al. 2011) suggests that new desorption pathways should be opened by photodissociation. Photodesorption initiated by molecular photodissociation is known to dominate in the case of H_2O. Molecular dynamics simulations on the photodesorption of H_2O ice (Andersson & van Dishoeck 2008; Andersson et al. 2011) have suggested a kick-out mechanism by energetic H fragments. This mechanism could be generalized to other molecules such as CH_4 that produce energetic fragments, including H, when photodissociated. Another possible process is where desorption occurs as the fragments of a molecule that dissociated, immediately recombine (geminate or direct recombination). Recombination can also occur for fragments coming from different molecules (secondary recombination); the fact that fragments are very energetic means that in condensed phase, they can travel far on the surface and in the bulk and react with other fragments. Such a process has been shown to exist for the UV photodesorption of O_2 (Fayolle et al. 2013) and CO_2 (Fillion et al. 2014; Martín-Doménech et al. 2015). Another indication that photodissociation and subsequent radical chemistry likely plays an important role in CH_4 desorption, is the desorption of heavier hydrocarbons such as C_2H_4 observed by Cruz-Diaz (2015) upon VUV irradiation of CH_4 ice.

One interesting piece of information that we can extract from our data is where the energy goes when photons are absorbed at the surface of the ice. The final outcomes of the initial event of a photon being absorbed by a molecule near the surface can be divided into three channels. Two measurable channels are (i) a CH_4 desorption event and (ii) the effective destruction of a CH_4 molecule. It should be noted that the second channel does not characterize photodissociation, since photodissociation can also lead to desorption or recombination into a CH_4 molecule. Rather, this outcome corresponds to photochemistry; radicals and/or photoproducts are created. The third is then (iii) the energy is relaxed through various pathways. The weight of this third channel can be deduced from the quantification of the initial step and the first two outcomes. The absorption cross-section of pure solid CH_4 at Lyman-α (10.2 eV) has been measured by Cruz-Diaz et al. (2014b) as 1.5×10^{-17} cm^2. Assuming that desorption occurs in the first three monolayers of the ice, we find a photodesorption yield of ~0.05 molecules desorbed per absorbed photon at Lyman-α. This value characterizes channel (i). Öberg et al. (2010) evaluated the effective photodestruction cross-section of pure CH_4 ice irradiated by a Lyman-α dominated discharge lamp as 5×10^{-19} cm^2, which corresponds to ~0.033 destroyed molecules per absorbed photons. We can consider this value to represent channel (ii) if we make the hypothesis that photodestruction is similar at the surface and in the bulk. Both values derived for channels (i) and (ii) are low and suggest that channel (iii) dominates; most of the absorbed energy is relaxed away.

These values can be compared with the photodesorption yields per absorbed photon derived by Cruz-Diaz et al. (2014a) for CO, which are above unity for all wavelengths, meaning that each photon absorption leads on average to one or even multiple desorption events. The energetics in these two cases are therefore very different. The photodesorption yield per absorbed photon of CH_4 is closer to the one found in Cruz-Diaz et al. (2014b) for O_2, another molecule where photodesorption has been linked to photodissociation.

Table 1. $^{13}CH_4$ photodesorption yields per incident photon for pure CH_4 ice in various interstellar environments.

	Dense cores[a]	Protoplanetary disks[b]	ISRF[c]
	($\times 10^{-3}$ molecules/photon)		
Pure CH_4	2.2 ± 1.1	2.2 ± 1.1	2.0 ± 1.0

Notes. UV fields are taken from [(a)] Gredel et al. (1987); [(b)] Johns-Krull & Herczeg (2007); and [(c)] Mathis et al. (1983).

4.2. Desorption induced by CO molecules

The results obtained on layered CH_4:CO ices provide some insight into CO-induced desorption. In a previous study, N_2 overlayer desorption induced by the underlying CO ice excitation has been shown to be a very efficient process (Bertin et al. 2012). Indeed, the photodesorption yield of N_2 can reach up to ~2.5×10^{-2} molecule/photon at a photon energy of 8.3 eV when it is adsorbed onto CO ice, whereas it is almost zero when N_2 is pure. As can be seen in Fig. 2, the CH_4 desorption induced by the CO excitation barely reaches 2×10^{-3} molecule/photon at the same energy. It is interesting, therefore, to discuss this difference of one order of magnitude as compared with the case of N_2. The efficiency of the indirect process for different molecules can be driven by several parameters corresponding to the different steps of the mechanism: the inter-molecular energy transfer, the intra or inter-molecular energy relaxation once it has been transferred, and the binding energy of the molecule. CH_4 is as volatile as CO and N_2, and although no data is available on the CH_4-CO binding energy to our knowledge, it is reasonable to assume that it would not be very different from the CH_4 binding energy with itself (~100 meV, Smith et al. 2016). If the energy transfer is simply a kinetic momentum transfer, since CH_4 is lighter than N_2 or CO, we would expect the transfer to be even more efficient. However, a good case can be made for the limiting step being intra or inter-molecular energy relaxation. Aside from a higher density of vibrational states into which energy can be partitioned, vibrational relaxation of polyatomic molecules is usually much faster than for diatomic molecules, due to the availability of relaxation pathways involving multiple vibration modes that do not exist for diatomic molecules (Nitzan 2006). Such an explanation also fits with the observed fact that in CH_3OH:CO ice mixtures, CO-induced desorption of CH_3OH is not observed (Bertin et al. 2016). Further investigations will aim at determining precisely what parameter(s) drive the efficiency of this process.

5. Astrophysical implications

5.1. Photodesorption yields of CH_4 from interstellar icy grains

By multiplying the photodesorption spectra we obtained with typical UV fields (with their integral normalized to unity) of different regions of the interstellar medium, we can derive average photodesorption yields for each of these regions. Table 1 gives such values for the dense core UV field calculated by

Gredel et al. (1987), the protoplanetary disk field calculated by Johns-Krull & Herczeg (2007) and the interstellar radiation field (ISRF) estimated by Mathis et al. (1983). The UV field in dense cores and the regions of protoplanetary disks far away from the star comes from secondary UV photons generated by cosmic rays, and is dominated by Lyman-α photons (at 10.2 eV). The photodesorption of CH_4 being relatively efficient at Lyman-α (Fig. 1), the average desorption yield for those environments is equal to the desorption yield at Lyman-α (Table 1 and Fig. 1). For the ISRF, where there is a higher contribution of lower-energy photons that do not efficiently photodesorb CH_4, the average desorption yield is slightly lower. These photodesorption yields are obtained for $^{13}CH_4$, but, considering the weak difference in mass, we expect about the same values for the $^{12}CH_4$ isotope.

We must, however, discuss the conditions of validity of these yields. They will depend on the accuracy of the UV field models for the considered region of the ISM, but also on how well our experimental conditions can be extrapolated to astrophysical ice mantles. They are thus only entirely valid for pure, thick ices of methane deposited at 10 K, that have not been further processed. "Thick" in the context of photodesorption experiments can be taken as a few tens of monolayers. Photodesorption is a surface process that mostly involves the first few monolayers of the ice, and although deeper layers can play a role to some extent, 20 monolayers can thus be considered "thick". The data obtained for 1 ML and 3 ML of CH_4 deposited on CO ice suggest, however, a thickness dependence of the photodesorption yields for thinner layers. Another factor that can affect photodesorption is ice morphology. Ice morphology is also linked to the deposition temperature of the ice in experiments and post-processing by UV photons or cosmic ray analogs, as has been extensively studied in the case of H_2O (e.g., Dartois et al. 2013, and references therein). A recent study by Muñoz Caro et al. (2016) has highlighted the influence of the physical properties of the CO ice on photodesorption: desorption yields for CO ices deposited between 7 and 20 K vary by up to a factor of 4. This effect has been attributed to the disorder of CO molecular dipoles affecting the energy transfer between molecules, and thus hindering the indirect desorption process mentioned in Sect. 3.2.

Another important aspect to take into account is the molecular environment; CH_4 is not found pure in ice mantles. Observations (Boogert et al. 2015) and models (Garrod & Pauly 2011) currently point to a two-phase model of interstellar ices: One H_2O-rich phase, formed when hydrogenation of atoms is a dominant process and containing NH_3, CH_4 and CO_2, and one CO-rich phase containing CH_3OH and CO_2. According to this model, an astrophysically realistic situation would therefore rather be CH_4 in a water matrix, containing other elements such as NH_3 and CO_2. In a first approximation, the yields obtained for pure ices can be extrapolated to an astrophysical ice by simply weighing each yield by the relative abundance of the species. However, a different environment means different binding energies, relaxation dynamics, and chemistry, all of which can significantly affect photodesorption – not to mention indirect desorption induced by different molecules. The latter is evidenced by our studies of desorption induced by CO. A more realistic case that still needs to be studied is the photodesorption of methane from an H_2O-rich ice. The relative parts of desorption, destruction, and relaxation are likely to change in a water matrix, although it is hard to predict in which way desorption will be affected. Experiments by Öberg et al. (2010) show a much increased photodestruction cross-section for CH_4 mixed with H_2O, while experiments on CO deposited on amorphous solid water (ASW) showed a decreased photodesorption, attributed to the ability of dangling OH from the water matrix to evacuate energy into the bulk very efficiently (Bertin et al. 2012). A recent study by Martín-Doménech et al. (2016) on the photodesorption of CH_4:H_2O ices only showed the desorption of reaction products (CO and H_2CO) initiated by the methane photodissociation. In this case, the desorption yield of intact CH_4 from a H_2O-rich ice has not been measured. More experiments, which await further beamtime, will be required to investigate all these considerations and to quantify all these effects on the CH_4 photodesorption yields from a water-rich or a CO-rich environment.

5.2. Solar system

As mentioned in Sect. 1, photodesorption may also be relevant in astrophysical contexts other than the ice mantles of interstellar grains, for example in the solar system. CH_4 is classified among the supervolatile molecules. In the ultra-high vacuum conditions of our experimental set-up, its sublimation temperature is around 30 K. Therefore, non-thermal desorption will likely only matter for the coldest regions of the solar system, in places where the ice is never exposed to solar light and photodesorption occurs because of the interstellar UV photons and the solar UV photons scattered by the interplanetary medium. For example, a scenario was recently published (Grundy et al. 2016) where the red color of the poles of Charon observed by New Horizons are suggested to originate from products of the photolysis of condensed CH_4 by the back-scattered solar UV photons. The CH_4 in this scenario comes from the evaporation of Pluto and is continuously deposited on Charon and trapped at the poles where the temperature is low enough for its condensation. This is a typical case where thermal desorption does not occur and non-thermal desorption pathways may thus play a role in the gas/ice dynamics. While in this precise case, the deposition rate ($\sim 2 \times 10^8$ molecules cm^{-2} s^{-1}) is much higher than the photodesorption rate expected considering the measured VUV flux (3.5×10^7 photons cm^{-2} s^{-1} with mostly Lyman-α photons would mean $\sim 7.7 \times 10^4$ desorbed molecules cm^{-2} s^{-1}), this scenario, as suggested by its authors, may be extended to other, smaller objects around Pluto. The example of Nix is taken, where the deposition rate is estimated to be 20 000 times lower than for Charon, in which case photodesorption would probably start being significant.

6. Conclusions

Pure amorphous CH_4 ices at 10 K were irradiated with synchrotron light (91–177 nm – 7–13.6 eV), and spectrally-resolved absolute CH_4 photodesorption yields were measured. These yields strongly depend on the wavelength, with no desorption below $\approx$136 nm. Photodesorption yields were derived for pure CH_4 ices for various astrophysical environments: for dense cores and disks they were found to be $2.2 \pm 1.1 \times 10^{-3}$ molecules per incident photon, equal to the value at Lyman-α energy, and for diffuse ISM conditions a value of $2.0 \pm 1.0 \times 10^{-3}$ molecules per incident photon was found. These yields can be added to models, keeping in mind the limits of their validity as has been discussed. Thin layered ices were also studied (1 ML of CH_4 above CO ice), and gave a different CH_4 photodesorption spectrum, with spectral signatures from both CH_4 and CO. This showed that both direct (i.e., the molecule absorbing a VUV photon is the one desorbing) and indirect (i.e., the molecule absorbing a VUV photon is not necessarily the one desorbing) electronic induced desorption mechanisms are at play. Comparison of CO-induced

desorption in the case of CH_4 with previously studied molecules allowed for discussion of the parameters driving this indirect process.

Acknowledgements. We acknowledge SOLEIL for provision of synchrotron radiation facilities under the project 20150760 and we would like to thank Laurent Nahon for assistance on the beamline DESIRS. This work was supported by the French program "Physique et Chimie du Milieu Interstellaire" (PCMI) funded by the Centre National de la Recherche Scientifique (CNRS) and Centre National d'Études Spatiales (CNES). Financial support from the LabEx MiChem, part of the French state funds managed by the ANR within the investissements d'avenir program under reference ANR-11-10EX-0004-02 is acknowledged. Fundings by the Ile-de-France region DIM ACAV program is gratefully acknowledged.

References

Aikawa, Y., & Nomura, H. 2006, ApJ, 642, 1152
Andersson, S., & van Dishoeck, E. F. 2008, A&A, 491, 907
Andersson, S., Arasa, C., Yabushita, A., et al. 2011, Phys. Chem. Chem. Phys., 13, 15810
Au, J. W., Cooper, G., Burton, G. R., Olney, T. N., & Brion, C. E. 1993, Chem. Phys., 209
Baratta, G., Domingo, M., Ferini, G., et al. 2003, Nuclear Instruments and Methods in Physics Research Section B: Beam Interactions with Materials and Atoms, 209, 283
Bennett, C. J., Jamieson, C. S., Osamura, Y., & Kaiser, R. I. 2006, ApJ, 653, 792
Bennett, C. J., Pirim, C., & Orlando, T. M. 2013, Chem. Rev., 113, 9086
Bertin, M., Fayolle, E. C., Romanzin, C., et al. 2012, Phys. Chem. Chem. Phys., 14, 9929
Bertin, M., Fayolle, E. C., Romanzin, C., et al. 2013, ApJ, 779, 120
Bertin, M., Romanzin, C., Doronin, M., et al. 2016, ApJ, 817, L12
Boogert, A. C. A., Helmich, F. P., Van Dishoeck, E. F., et al. 1998, A&A, 336, 352
Boogert, A. C. A., Blake, G. A., & Öberg, K. 2004, ApJ, 615, 344
Boogert, A., Gerakines, P., & Whittet, D. 2015, ARA&A, 53, 541
Bossa, J.-B., Paardekooper, D. M., Isokoski, K., & Linnartz, H. 2015, Phys. Chem. Chem. Phys., 17, 17346
Cleeves, L. I., Bergin, E. A., Alexander, C. M. O., et al. 2016, ApJ, 819, 13
Cruz-Diaz, G. A. 2015, Ph.D. Thesis, Universidad Autonoma de Madrid, Spain
Cruz-Diaz, G. A., Muñoz Caro, G. M., Chen, Y.-J., & Yih, T.-S. 2014a, A&A, 562, A119
Cruz-Diaz, G. A., Muñoz Caro, G. M., Chen, Y.-J., & Yih, T.-S. 2014b, A&A, 562, A120
Cruz-Diaz, G. A., Martín-Doménech, R., Muñoz Caro, G. M., & Chen, Y.-J. 2016, A&A, 592, A68
Dartois, E., d'Hendecourt, L., Boulanger, F., et al. 1998, A&A, 331, 651
Dartois, E., Ding, J. J., de Barros, A. L., et al. 2013, A&A, 557, A97
de Barros, A. L. F., Bordalo, V., Seperuelo Duarte, E., et al. 2011, A&A, 531, A160
Doronin, M., Bertin, M., Michaut, X., Philippe, L., & Fillion, J.-H. 2015, J. Chem. Phys., 143, 084703
Fayolle, E. C., Bertin, M., Romanzin, C., et al. 2011, ApJ, 739, L36
Fayolle, E. C., Bertin, M., Romanzin, C., et al. 2013, A&A, 556, A122
Fillion, J.-H., Fayolle, E. C., Michaut, X., et al. 2014, Faraday Discussions, 168, 533
Gans, B., Boyé-Péronne, S., Broquier, M., et al. 2011, Phys. Chem. Chem. Phys., 13, 8140
Garrod, R. T., & Pauly, T. 2011, ApJ, 735, 15
Gredel, R., Lepp, S., & Dalgarno, A. 1987, ApJ, 323, L137
Grundy, W. M., Cruikshank, D. P., Gladstone, G. R., et al. 2016, Nature, 539, 65
Hama, T., Yokoyama, M., Yabushita, A., et al. 2009, J. Chem. Phys., 131, 224512
Hassel, G. E., Herbst, E., & Garrod, R. T. 2008, ApJ, 681, 1385
Himpsel, F.-J., Schwentner, N., & Koch, E. E. 1975, Phys. Stat. Sol. (b), 71, 615
Hiraoka, K., Miyagoshi, T., Takayama, T., Yamamoto, K., & Kihara, Y. 1998, ApJ, 498, 710
Hodyss, R., Johnson, P. V., Stern, J. V., Goguen, J. D., & Kanik, I. 2009, Icarus, 200, 338
Hodyss, R., Howard, H. R., Johnson, P. V., Goguen, J. D., & Kanik, I. 2011, Icarus, 214, 748
Hollenbach, D., Kaufman, M. J., Bergin, E. A., & Melnick, G. J. 2009, ApJ, 690, 1497
Hudson, R. L., Gerakines, P. A., & Loeffler, M. J. 2015, Phys. Chem. Chem. Phys., 17, 12545
Johns-Krull, C. M., & Herczeg, G. J. 2007, ApJ, 655, 345
Johnson, R. E., Carlson, R. W., Cassidy, T. A., & Fama, M. 2013, in The Science of Solar System Ices, eds. M. S. Gudipati, & J. Castillo-Rogez, 356 (New York: Springer), 551
Kaiser, R. I., & Roessler, K. 1998, ApJ, 503, 959
Kalvans, J. 2015, ApJ, 803, 52
Kameta, K., Kouchi, N., Ukai, M., & Hatano, Y. 2002, J. Electron Spectrosc. Related Phenom., 123, 225
Koch, E.-E., & Skibowski, d. M. 1971, Chem. Phys. Lett., 9, 429
Kunz, A. B. 1983, Phys. Rev. B, 28, 3465
Lo, J.-I., Lin, M.-Y., Peng, Y.-C., et al. 2015, MNRAS, 451, 159
Maity, S., Kaiser, R. I., & Jones, B. M. 2014, ApJ, 789, 36
Martín-Doménech, R., Manzano-Santamaría, J., Muñoz Caro, G. M., et al. 2015, A&A, 584, A14
Martín-Doménech, R., Muñoz Caro, G. M., & Cruz-Díaz, G. A. 2016, A&A, 589, A107
Mathis, J. S., Mezger, P. G., & Panagia, N. 1983, A&A, 128, 212
Milligan, D. E., & Jacox, M. E. 1967, J. Chem. Phys., 47, 5146
Mumma, M. J., & Charnley, S. B. 2011, ARA&A, 49, 471
Muñoz Caro, G. M., Chen, Y.-J., Aparicio, S., et al. 2016, A&A, 589, A19
Nahon, L., de Oliveira, N., Garcia, G. A., et al. 2012, J. Synch. Radiat., 19, 508
Nitzan, A. 2006, Chemical dynamics in condensed phases: relaxation, transfer and reactions in condensed molecular systems, Oxford graduate texts (Oxford, New York: Oxford University Press)
Robin, M. B. 1974, Higher excited states of polyatomic molecules (New York: Acad. Press)
Romanzin, C., Gazeau, M.-C., Bénilan, Y., et al. 2005, Adv. Space Res., 36, 258
Ruaud, M., Wakelam, V., & Hersant, F. 2016, MNRAS, 459, 3756
Sakai, N., & Yamamoto, S. 2013, Chem. Rev., 113, 8981
Smith, N. S., & Raulin, F. 1999, J. Geophys. Res.: Planets, 104, 1873
Smith, R. S., May, R. A., & Kay, B. D. 2016, J. Phys. Chem. B, 120, 1979
Tian, C., & Vidal, C. R. 1998, J. Phys. B: At. Mol. Opt. Phys., 31, 895
Wu, Y.-J., Wu, C. Y. R., Chou, S.-L., et al. 2012, ApJ, 746, 175
Yuan, C., & Yates, J. T. 2014, ApJ, 780, 8
Öberg, K. I., Boogert, A. C., Pontoppidan, K. M., et al. 2008, ApJ, 678, 1032
Öberg, K. I., van Dishoeck, E. F., & Linnartz, H. 2009, A&A, 496, 281
Öberg, K. I., van Dishoeck, E. F., Linnartz, H., & Andersson, S. 2010, ApJ, 718, 832